Journal of Catalysis **212,** 10–21 (2002)
doi:10.1006/jcat.2002.3739

Characterization of Alumina, Silica, and Titania Supported Cobalt Catalysts

M. Voß, D. Borgmann,[1] and G. Wedler

Institute of Physical and Theoretical Chemistry, University of Erlangen-Nürnberg, Egerlandstr. 3, D-91058 Erlangen, Germany

Received April 10, 2002; revised June 20, 2002; accepted June 27, 2002

A multiple technique approach was used to characterize the structural, chemical, and electronic properties of Co catalysts supported on Al_2O_3, SiO_2, and TiO_2 as well as Co/Mn catalysts on TiO_2. The morphology of the catalysts was studied by transmission electron microscopy followed by X-ray diffraction to determine the phase composition and the distribution of the crystallite size. The electronic properties of the calcined catalysts were investigated by X-ray photoelectron spectroscopy. Comparison with reference data allows identification of the cobalt-containing species in the surface. In agreement with adsorption experiments, the signal intensities yield the dispersion of the applied catalysts in the sequence $Co/Al_2O_3 > Co/TiO_2 > Co/SiO_2$. Temperature-programmed reduction and oxidation reveal the formation of various oxides in dependence on temperature as well as, in case of the alumina- and titania-supported cobalt catalysts, the formation of high-temperature compounds $CoAl_2O_4$ and $CoTiO_3$, respectively. Dynamic and static adsorption studies and BET measurements complete the characterization of the supported catalysts.

Key Words: **cobalt; manganese; alumina; silica; titania; supported catalysts; electron microscopy; X-ray diffraction; photoelectron spectroscopy; temperature-programmed reduction and oxidation; dynamic and static adsorption studies.**

1. INTRODUCTION

The bridging of the pressure and materials gap in surface science and heterogeneous catalysis has been a large challenge for some decades. Many attempts were made to bridge the pressure gap between ultrahigh vacuum conditions and reaction conditions in the mbar and bar regimes by means of *in situ* (1–3) and *ex situ* studies (4). On the other hand, it is just as important to overcome the materials gap, i.e., to pass from well-defined single crystals in basic research to more real catalysts such as the supported catalysts used in heterogeneous technical catalysis.

Supported cobalt catalysts play an important role in Fischer–Tropsch synthesis. During the past few years our group has performed extensive model studies of the adsorption of oxygen and water on Co(11$\bar{2}$0) single crystals (5–7) as well as the hydrogenation of CO_2 on polycrystalline Co foils (8, 9) and supported Co catalysts in order to gain better insight into both the activation and deactivation processes of the catalysts used and the product distribution of the hydrogenation reaction (10).

At first glance, polycrystalline Co foils and the supported Co catalysts prepared under identical conditions on Al_2O_3, SiO_2, and TiO_2 behave differently in the test reaction, the hydrogenation of CO_2, with regard to stability and activity. Therefore efforts were made to carry out detailed studies to elucidate the structural, chemical, and electronic properties of these catalysts.

The aim of these studies is (i) to characterize the morphological properties of the catalysts, (ii) to determine the phase composition in the bulk and at the surface, and (iii) to find out the dispersion of the Co containing species and the number of active sites. The investigation of the electronic properties (iv) and the influence of support and preparation on these properties (v) were further subjects of this study. In an additional paper, which is in preparation, it will be shown that the results of the present paper provide an explanation of the observed differences in the catalytic behavior of the supported Co catalysts in the hydrogenation of CO_2.

2. METHODS

2.1. Preparation of Supported Catalysts

The supported Co and Co/Mn catalysts were prepared at the Jagiellonian University in Cracow by means of incipient wetness impregnation. The supports were impregnated with $Co(NO_3)_2$ and $Mn(NO_3)_2$ solution, respectively, the concentration and volume of which correspond to the desired metal content of the catalysts (see Table 1). Then the samples were dried for 3 h at 403 K. Calcination occurred for 3 h at 873 K in an air current, whereby the nitrates thermally decomposed under formation of the oxides.

All experiments with calcined samples were performed with these materials. For experiments with reduced catalysts, the exact reduction conditions will be given in the corresponding paragraphs.

[1] To whom correspondence should be addressed. Fax: 0049-9131-8528867. E-mail: borgmann@pctc.chemie.uni-erlangen.de.

0021-9517/02 $35.00

TABLE 1

Specific Metal Contents of the Co Catalysts Used

Catalyst	Support	Weight% Co	Weight% Mn
Co/Al_2O_3	Al_2O_3, Degussa AG, Type: C	5.04	—
Co/SiO_2	SiO_2, Degussa AG, Type: Aerosil 200	4.71	—
Co/TiO_2	TiO_2, Degussa AG, Type: P25	5.22	—
$Co/Mn/TiO_2$	TiO_2, Degussa AG, Type: P25	6.27	2.67

2.2. Applied Methods

A multiple method approach has been used to study the structural and chemical properties of Co catalysts supported on Al_2O_3, SiO_2, and TiO_2 and of Co/Mn catalysts on TiO_2 in their states after calcining, reduction, and reoxidation.

2.2.1. Electron microscopy. To obtain a preliminary idea of the structural properties (crystalline, amorphous, particle size) of the catalysts, electron microscopy (SEM (Jeol JSM 6400), TEM (Phillips CM 200)) was applied in various modes (11). Since this method can be used only when the sample is thin enough ($\leq$100 nm), a special preparation technique had to be used. By means of the bright-field mode, a two-dimensional projection of the sample was obtained. Removal of the object aperture led to the appearance of the diffraction pattern of the whole sample, so that the chemical phase composition of the catalyst could be determined by comparison with the diffraction patterns of reference materials. When the electron beam was focused (diameter <4 nm) and scanned over the sample (scanning transmission electron microscopy, STEM) both a very clear bright-field image and a mapping of the spatial distribution of the chemical elements were obtained, and the X-ray fluorescence of the various elements was recorded (energy dispersive analysis of X-rays).

The samples were prepared for electron microscopy in the following way. A small amount of the catalyst was stirred together with a mixed adhesive (epoxy resin) of high viscosity. The resulting suspension was deposited on a fine mechanical copper net (thickness 40–50 μm, diameter about 3 mm). An increase in the temperature to 323 K led to a decrease in the viscosity of the suspension, so that the suspension was sucked into the meshes by capillary forces. When the temperature was increased to 393 K, the mixed adhesive cured. Then the solid material was mechanically abraded down to the thickness of the copper net. To obtain an even thinner sample, it was bombarded with a beam of Ar^+ ions (7 kV, 2 mA) at an angle of 8° against the surface. After sputtering (about 5 h) in the middle of the sample, a small hole was formed, the edge of which was thin enough to be permeable to a beam of high-energy electrons.

2.2.2. X-ray diffraction. To obtain information concerning the phase composition and the crystallite size distribution of the catalysts after the calcination, X-ray diffraction measurements (Fa. Huber) were performed. The powder diffraction records the exact position as well as the intensity of the diffraction peaks (by numerical integration after background subtraction). The phases were identified by comparison with literature data (12). Since the size of the cobalt oxide crystallites was smaller than 100 nm, broadening of the X-ray diffraction peaks was observed. Therefore it was possible to calculate the thickness of the crystallites by means of X-ray line broadening analysis (13, 14).

2.2.3. X-ray photoelectron spectroscopy (XPS). XPS experiments were carried out with a photoelectron spectrometer (Vacuum Generators, ESCALAB 200). The difficulty in fixing powdery samples on the sample holder of this equipment was overcome by pasting the sample on the holder with an electrically conducting silver suspension (Silver Print, Baltex). XPS measurements with samples of pressed pellets led to identical results. As far as possible the sample was dried and degassed in a desiccator cabinet at 150°C for 30 min, before it was put into the prevacuum chamber of the device, which was evacuated within 2 to 3 h down to a pressure of 10^{-6} mbar. Then the sample was transferred into the analytical chamber by means of a transfer sledge. During all measurements the residual gas pressure was lower than 5×10^{-10} mbar.

Due to the insulating character of the calcined oxidic samples, they become positively charged during the photoelectron emission process. The charging can amount to up to 10 eV. Therefore the C1s signal was used as an internal standard. This signal originates from carbonaceous species, which proved to be present in each of the samples investigated. The C1s binding energy was—in agreement with literature data—taken to be 284.8 eV.

Much attention was focused on the exact quantitative evaluation of the XPS intensities. A description of this procedure is not possible within the scope of this paper (for details see, e.g., Refs. 15–18). The determination of the dispersion of the supported particles followed the randomly oriented layer model according to Kuipers *et al.* (19, 20).

2.2.4. Temperature-programmed reduction (TPR) and oxidation (TPO). In temperature-programmed reduction or oxidation, a sample of the catalyst is heated in a stream of hydrogen or oxygen, respectively, with continuous measurement of the consumption of these gases by the reaction between gas and sample. It has been useful to apply diluted gas mixtures (in our case 10% O_2 in He and 8.99% H_2 in Ar, respectively). The large difference in the thermal conductivity of inert gas and reaction gas allows precise recording of the gas consumption as a function of temperature by means of a thermal conductivity cell. In reduction the water vapor formed has nearly the same thermal

conductivity as the carrier gas Ar and in oxidation no gaseous product is formed, so that the change in thermal conductivity is proportional to the amount of hydrogen and oxygen consumed, respectively. The area below the curve plotted by the thermal conductivity cell has the dimension signal × temperature. When the temperature changes linearly with time ($\beta = dT/dt$), it can easily be transformed into an integral with the dimension signal × time. Calibration occurs by injection of a known amount of Ar or He, respectively, into the H_2/Ar or O_2/He mixture or vice versa.

The measurements were performed with an AMI-100 device (Altamira). Fifty to one hundred milligrams of the calcined catalyst was filled into the sample holder. The sample was thoroughly degassed in a stream of He or Ar, respectively, before the TPR or TPO measurement was started. Degassing occurred in both cases during an increase and decrease in temperature between 323 and 573 K (±30 K/min). During reduction and oxidation the temperature was increased from 323 to maximally 1323 K (10 K/min).

2.2.5. Dynamic adsorption studies. The experiments were performed with the AMI-100 device (Altamira), which had already been used in the TPR and TPO experiments. Samples of 50 to 100 mg were used and isothermally reduced at 673 K for 120 min ($v = 25$ ml/min). Oxidation occurred by O_2 pulses admitted to the stream of He. The experiments described here were carried out at 673 K, oxidation in 0.1 vol% O_2 in nitrogen for 30 min, reduction in pure hydrogen for 600 min, and conservation up to the catalytic process at 300 K in pure helium. In every case the velocity of the gas stream was 15 ml/min.

2.2.6. Static adsorption experiments. To determine the whole surface of the sample by means of BET measurements (21) or the number of active centers on the metal surface by means of selective adsorption, ASAP 2010C adsorption equipment (Micromeritics) was used, which allowed special pretreatments of the sample. BET experiments followed the usual procedure. In the case of selective adsorption, an adsorption isotherm was measured at a temperature considerably below the desorption temperature of the chemisorbed species. Evacuation removed only the physisorbed amount. Only this amount could be readsorbed, when a second adsorption isotherm was measured. The difference of the two adsorption isotherms represents the chemisorbed amount, which yields under distinct assumptions the number of active centers.

3. RESULTS AND DISCUSSION

3.1. Results Obtained by Means of Electron Microscopy

It should be kept in mind that the sample investigated by electron microscopy consists of the catalyst in the calcined state. To what extent the results are also representative of the catalyst in the reduced or in the reoxidized state can be decided only when comparison with corresponding results obtained with other methods becomes possible.

Figure 1a shows a TEM image of the Co/SiO_2 catalyst. Dark crystalline spots can be observed beside bright amorphous regions. Due to the strong mass differences between Si and Co it can be assumed that the dark spots indicate Co oxide crystallites, which are embedded into amorphous SiO_2.

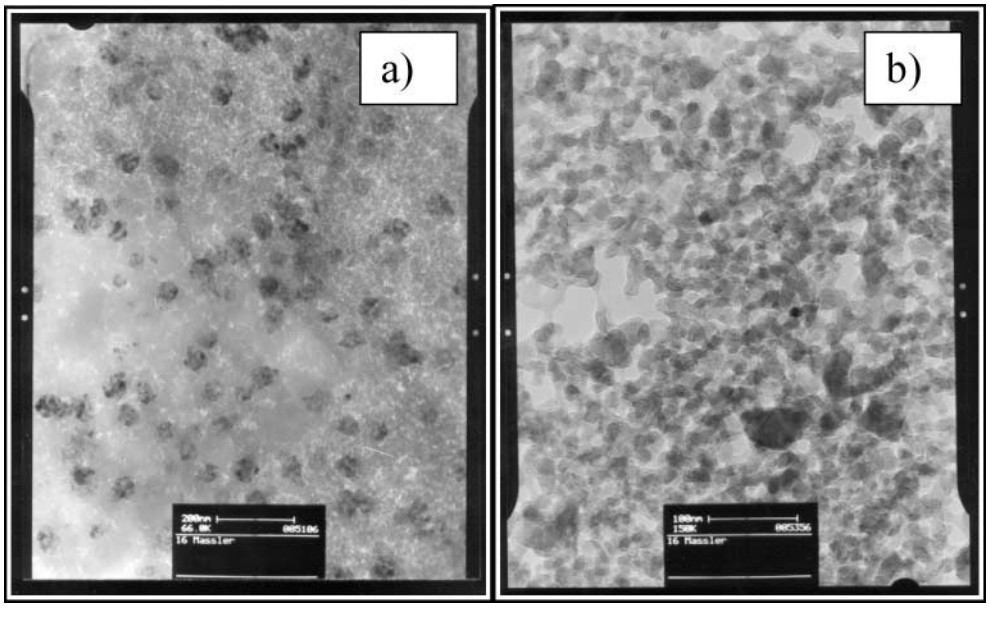

FIG. 1. Transmission electron micrographs of (a) a Co/SiO_2 catalyst and (b) a Co/Al_2O_3 catalyst in bright field. The magnification factors of the original image are 66,000 and 150,000, respectively.

TABLE 2

Comparison of Experimentally Determined Lattice Distances of Co/TiO_2 and $Co/Mn/TiO_2$ Catalysts with Literature Data of CoO (12)

Co/TiO_2 and $Co/Mn/TiO_2$		CoO	
(*hkl*)	*d* (Å)	*d* (Å)	Rel. intensity
(111)	2.47	2.460	75
(200)	2.13	2.130	100
(220)	1.51	1.506	50
(311)	1.29	1.285	20
(222)	1.22	1.230	16
(400)	1.06	1.065	10
(420)	0.95	0.953	30

The Co/Al_2O_3 catalyst in Fig. 1b gives quite another TEM image. Both the cobalt oxide and the support material reveal a crystalline structure, but it is not possible to distinguish between the two components. The Co/TiO_2 catalyst (Figure not shown in this paper) exhibits a TEM image similar to that of the Co/Al_2O_3 catalyst. It is also evident that the Co/TiO_2 catalyst is crystalline. Since on one hand the atomic masses of Co and Ti do not differ considerably from one another (i.e., there is no remarkable mass contrast) and on the other hand the brightness or darkness of an item in a TEM image depends on its orientation, it is not possible to distinguish which items belong to the Co component and which belong to the support material.

Additional information on the phase composition of the samples is given by the electron diffraction patterns. They consist of rings with superimposed diffraction spots. In the case of the Co/SiO_2 catalyst, evaluation and comparison with literature data (12) reveal that the dark spots can be attributed to Co_3O_4, while in the case of the Co/Al_2O_3 catalyst the fine range diffraction patterns reveal crystalline γ-Al_2O_3 support besides crystalline CoO. Neither the Co/Al_2O_3 nor the Co/TiO_2 catalyst shows a Co_3O_4 phase, which is exclusively observed in the Co/SiO_2 catalyst. In the Co/TiO_2 samples the pictures are dominated by diffraction patterns showing the presence of the TiO_2 modifications rutile and anatase. There are, however, also fine range diffraction patterns which indicate the existence of cobalt oxide crystals, in the Co/TiO_2 catalyst as well in the $Co/Mn/TiO_2$ catalyst. The interplanar spacing *d* calculated from the diameters of the diffraction rings are nearly identical with the values found in the literature (12) for Co(II)-oxide CoO. Table 2 summarizes the diffraction parameters of CoO determined for the Co/TiO_2 and $Co/Mn/TiO_2$ samples, respectively.

Information on the spatial distribution of the cobalt oxide in the support can be obtained from a combination of scanning electron microscopy and element mapping using Co $K\alpha$ and Ti $K\alpha$ X-ray fluorescence of the support, respectively. Figures 2a–2c show the STEM image, the Co, and the

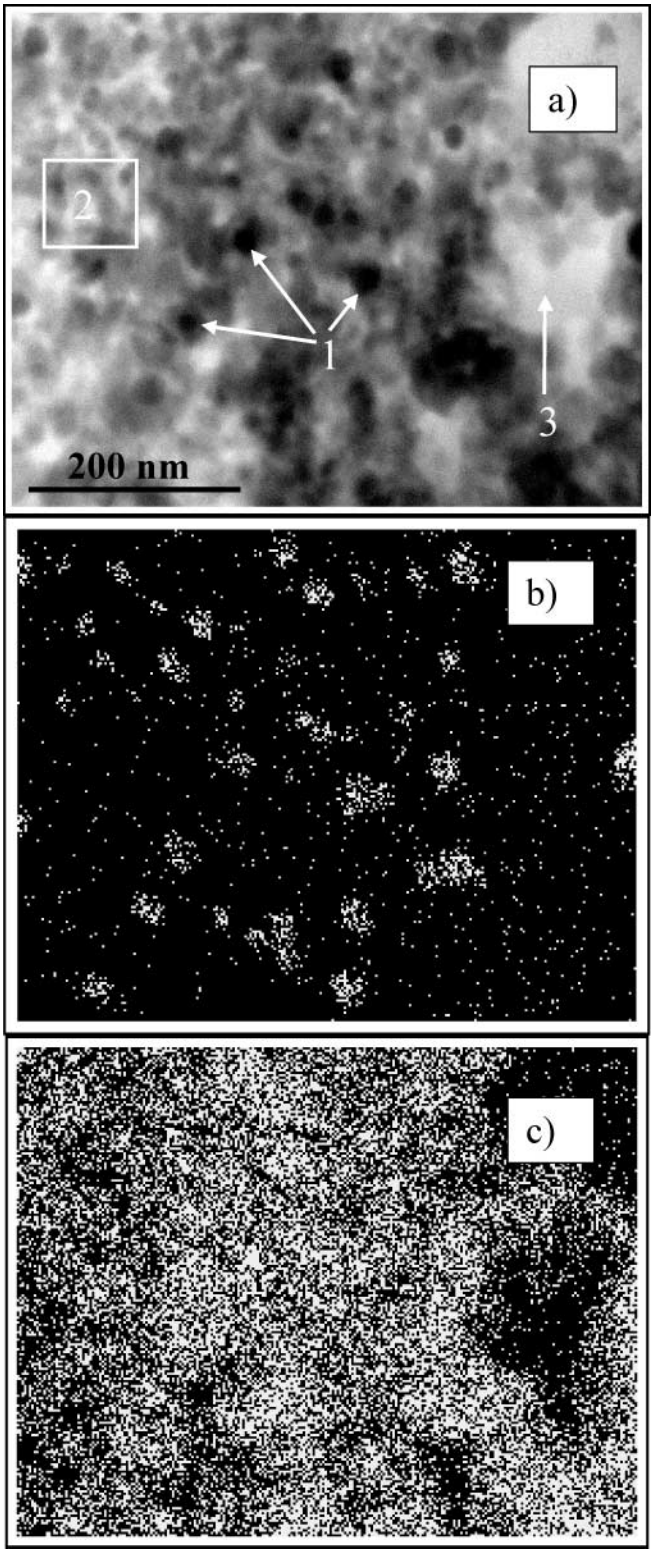

FIG. 2. (a) STEM image of Co/TiO_2, magnification factor 200,000; (b) Co $K\alpha$ mapping of a, and (c) Ti $K\alpha$ mapping of a.

Ti $K\alpha$ mapping of the Co/TiO_2 catalyst. In the TEM image (Fig. 2a) three characteristic ranges, 1–3, have been marked. Comparison with Figs. 2b and 2c shows that rather dark regions in Fig. 2a indicate the presence of cobalt oxide, the less dark crystals that of anatase or rutile. Since in regions 1 the Ti $K\alpha$ X-ray fluorescence is not markedly reduced in comparison with regions 2, the small CoO crystals must be embedded into the matrix of the support. Range 3, where neither Co nor Ti is present, points to the presence of the epoxy resin. This interpretation is supported by the total X-ray fluorescence spectra taken from the different regions over the energy range from 0 to 10 keV.

The electron microscopic methods indicate that the calcined catalysts consist of different crystalline and amorphous phases. Co/Al_2O_3 shows a homogeneous distribution of the elements Al and Co in the crystalline phases γ-Al_2O_3 and CoO, while the Co in the Co/SiO_2 catalyst can be attributed to Co_3O_4, which is embedded into amorphous SiO_2. The Co/TiO_2 catalyst consists of crystalline anatase and rutile as support material on which small CoO crystallites are distributed.

3.2. Results Obtained by Means of X-Ray Diffraction

Figure 3a shows the powder X-ray diffraction patterns of Co/SiO_2. The signals confirm the results of the TEM investigations that only Co_3O_4 is present as crystalline phase; SiO_2 is amorphous. Figure 3b presents the powder X-ray diffraction patterns of the $Co/Mn/TiO_2$ catalyst. The rather complex diffraction patterns point to a superposition of the X-ray diagrams of various substances. Indeed, the signals of Fig. 3b can be attributed to the two TiO_2 modifications anatase and rutile. In addition, diffraction peaks of cobalt titanate ($CoTiO_3$), but not those of a manganese containing phase, can be unambiguously observed, as follows from Table 3. This compound must have been formed from TiO_2 and divalent CoO during the calcination process.

In contrast to Co/SiO_2 and Co/Al_2O_3, in the X-ray diffraction patterns of Co/TiO_2 and $Co/Mn/TiO_2$ catalysts it was not possible to detect signals originating from CoO or Co_3O_4. An explanation of this observation could be that the cobalt oxide signals are hidden behind the titanium oxide signals of strong intensity. Evaluation of the Co/Al_2O_3 diffraction results reveals that the data mainly fit γ-Al_2O_3. Additional signals close to the γ-Al_2O_3 signals point to the presence of the spinell $CoAl_2O_4$ (Thénards' Blue), which has likely been formed during the calcination procedure at high temperatures.

The calculation of the thickness of the crystallites by means of X-ray line broadening analysis (13, 14) delivers for the cobalt oxide on the Al_2O_3 support a crystallite diameter of 20–25 nm (under the assumption of spherical crystallites). The value for the cobalt oxide on SiO_2 is 47 nm, calculated from the FWHM of the (311) and (440) reflections (Fig. 3a), and that for the cobalt oxide on TiO_2 amounts to about 30 nm, determined by TEM.

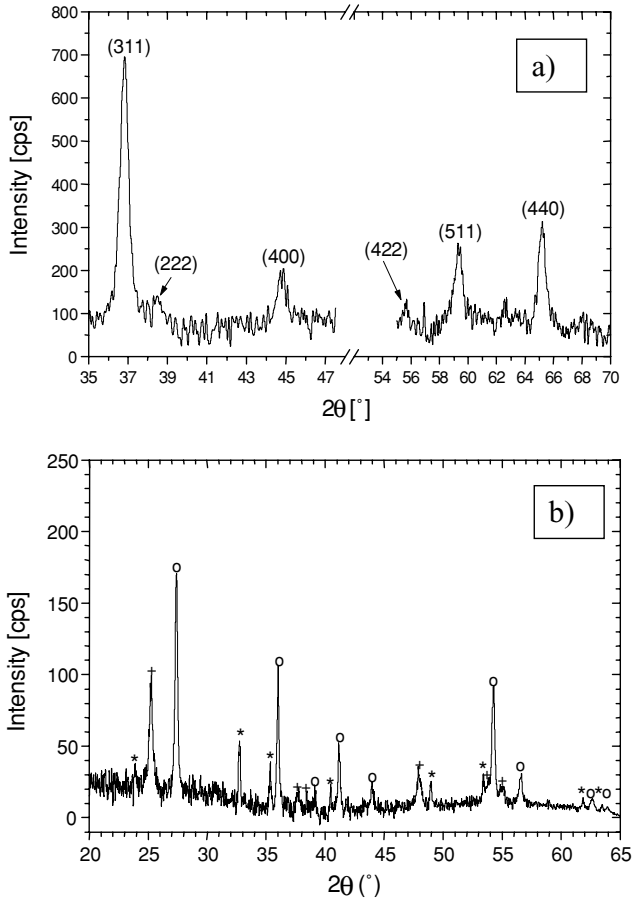

FIG. 3. X-ray diffraction patterns of the (a) Co/SiO_2 catalyst showing only reflections of Co_3O_4 and (b) $Co/Mn/TiO_2$ catalyst showing the reflections of $+ = TiO_2$ (anatase), $\circ = TiO_2$ (rutile), and $* = CoTiO_3$.

3.3. Results Obtained by Means of X-Ray Photoelectron Spectroscopy

To be able to interpret the XP spectra of the calcined supported catalysts Co/Al_2O_3, Co/SiO_2, Co/TiO_2, and $Co/Mn/TiO_2$, the XP spectra of the pure supports Al_2O_3,

TABLE 3

Comparison of Experimentally Determined X-Ray Diffraction Parameters of the $Co/Mn/TiO_2$ Catalyst with Literature Data of $CoTiO_3$ (12)

	$Co/Mn/TiO_2$ catalyst			$CoTiO_3$	
(*hkl*)	2θ (°)	*d* (Å)	Rel. intensity	*d* (Å)	Rel. intensity
(012)	23.88	3.72	35	3.717	35
(104)	32.84	2.73	100	2.727	100
(110)	35.35	2.54	72	2.534	75
(113)	40.49	2.23	<30	2.224	25
(024)	48.98	1.86	36	1.857	30
(116)	53.42	1.71	40	1.711	40
(214)	61.88	1.50	—	1.497	25
(300)	63.50	1.46	—	1.463	30

SiO_2, and TiO_2, of the pure cobalt oxides CoO and Co_3O_4, and of the possible solid-state product $CoAl_2O_4$ were taken. General spectra of the calcined catalysts were collected for binding energies between 0 and 1100 eV to look for the presence of impurities. However, there was only a very small signal of C1s, which was used to calibrate the energy scale.

Figure 4a shows the Co 2p XP spectra of the calcined catalysts Co/Al_2O_3, Co/TiO_2, and Co/SiO_2. Since all spectra were collected under the same experimental conditions, the intensities of the signals indicate a direct measure for the degree of dispersion of the Co compounds. In agreement with the TEM and XRD results the dispersion decreases in the sequence $Co/Al_2O_3 > Co/TiO_2 > Co/SiO_2$. The main signals of the Co $2p_{3/2,1/2}$ doublet are separated by 15.7 eV in the case of Co/Al_2O_3 ($E_b = 780.7$ and 796.4 eV) and Co/TiO_2 ($E_b = 780.3$ and 796.0 eV), respectively, but only by 15.2 eV in the case of Co/SiO_2 ($E_b = 779.9$ and 795.1 eV). As the values in the parentheses show, the binding energy of the Co $2p_{3/2}$ signal decreases in the sequence $Co/Al_2O_3 > Co/TiO_2 > Co/SiO_2$. The peaks exhibit a shoulder at their high-energy side, which has to be traced back to a shake-up process. Such signals can only be observed with Co(II)compounds in the high spin state. The diamagnetic low-spin Co^{3+} ion does not show shake-up structures.

An exact assignment of the Co compounds on the supports is possible when reference spectra of pure CoO, Co_3O_4, and $CoAl_2O_4$ are compared in Fig. 4b. The Co binding energies in CoO (E_b(Co $2p_{3/2}$) = 780.0 eV, E_b(Co $2p_{1/2}$) = 795.9 eV), and in Co_3O_4 (E_b(Co $2p_{3/2}$) = 780.2 eV, E_b(Co $2p_{1/2}$) = 795.5 eV) are only slightly lower than those in the calcined catalyst, while the spinell $CoAl_2O_4$ (E_b(Co $2p_{3/2}$) = 781.5 eV, E_b(Co $2p_{1/2}$) = 797.2 eV) shows significantly higher binding energies. The slightly higher Co 2p binding energies in the catalysts Co/Al_2O_3 and Co/TiO_2 might be explained by a partial formation of $CoAl_2O_4$ and $CoTiO_3$, respectively. However, the intensity of the shake-up signals in Co_3O_4 is remarkably reduced in comparison to CoO in agreement with the Co^{3+}/Co^{2+} ratio of 2 : 1 in Co_3O_4. Therefore the XP spectra of Co/Al_2O_3 and Co/TiO_2 point to a preferred presence of CoO, whereas the Co 2p spectrum of the Co/SiO_2 catalyst demonstrates that the mixed-valent cobalt oxide Co_3O_4 is present.

As well as the structure the energetic positions of the Co signals of the calcined $Co/Mn/TiO_2$ catalyst (figure not shown) agree very well with those of the Co/TiO_2 catalyst. It is interesting to note that the intensities of the Mn 2p signals are very similar to those of the Co 2p signals despite the Mn content of the catalyst being only about 43% of that of Co and the cross section of Mn being only 73% of that of Co. This observation points to a higher degree of dispersion of Mn. The energetic position of the Mn $2p_{3/2}$ signal in the catalyst (E_b(Mn $2p_{3/2}$) = 640.2 eV) indicates that the calcined catalyst contains MnO. Higher states of oxidation would shift the signal to higher binding energies.

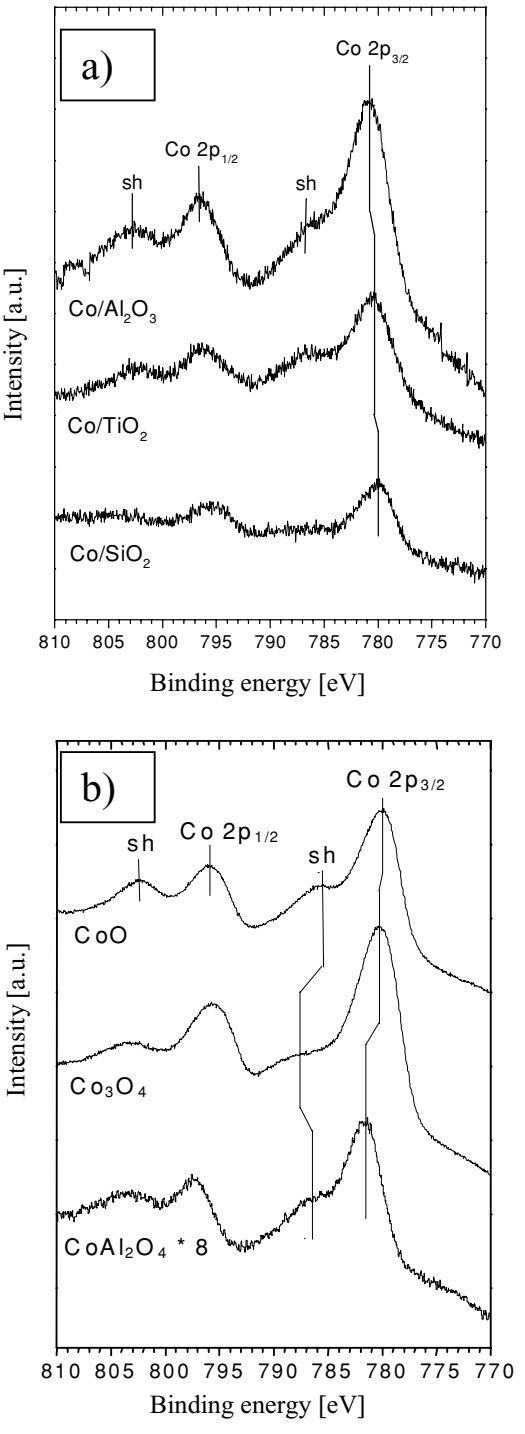

FIG. 4. Co2p XP spectra of (a) Co/Al_2O_3, Co/TiO_2, and Co/SiO_2 and (b) CoO, Co_3O_4, and $CoAl_2O_4$.

It should be mentioned that the photoelectron spectroscopic results show the composition of the surface and near-surface regime. However, these results agree well with the TEM and XRD data of the bulk regime, which reveal that

in the case of Co/Al_2O_3 and Co/TiO_2 catalysts mainly CoO is distributed on the crystalline support, while in the case of Co/SiO_2, Co_3O_4 is embedded in an amorphous support.

3.4. Results Obtained by Means of Temperature-Programmed Reduction and Oxidation

Electron microscopy, X-ray diffraction, and photoelectron spectroscopy yielded information on the properties of the supported Co catalysts after the calcination process. However, they did not give information on the properties of the reduced, catalytically active supported catalysts. The relation between the calcined, the reduced, and the reoxidized state of the supported catalysts as well as information on the formation and stability of the relevant phases can be investigated by means of temperature-programmed reduction and oxidation, which have been carried out with calcined samples of the three supported catalysts.

As an example, Figs. 5a and 5b show TPR experiments that were performed with Co/TiO_2 and $Co/Mn/TiO_2$ catalysts, respectively. With regard to the signal intensities in the figures, it must be noted that the amount of substance, the metal content, and the applied amplification differed in both experiments. There are only a few similarities between the curves in Figs. 5a and 5b. Both curves show the start of the reduction reaction at about 500 K and the end of the reaction above 1000 K. The structure of the curves points to the presence, partly to a superposition, of various reduction reactions.

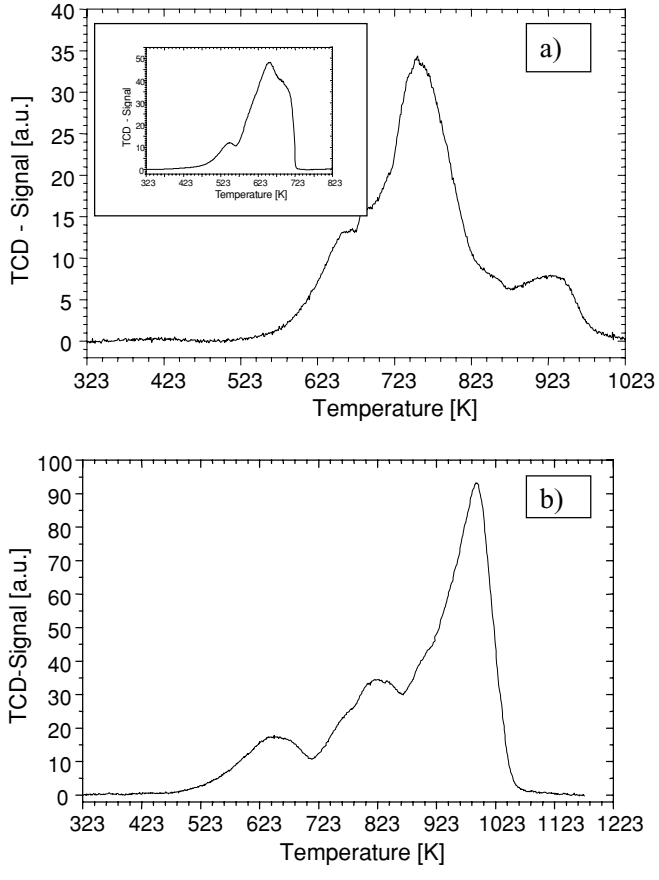

FIG. 5. TPR patterns of the (a) calcined Co/TiO_2 catalyst, pure Co_3O_4 (inset), and (b) calcined $Co/Mn/TiO_2$ catalyst.

To analyze the structures of the curves, it is necessary to compare them with structures of known substances that have been treated in the same way. The inset to Fig. 5a shows the TPR curve of pure Co_3O_4. Its first peak at 545 K must be attributed to the reduction of trivalent Co to divalent Co. The main signal at 650 K and the shoulder at 710 K can be traced back to the reduction of CoO to metallic Co.

At first glance there seems to be very poor overlap of the profile in Fig. 5a (inset) with the profiles in Figs. 5a and 5b, respectively. The situation changes completely when the calcined Co/TiO_2 and $Co/Mn/TiO_2$ catalysts are subjected to oxidation/reduction cycles, by which they are activated for catalytic reactions. After this treatment the differences between the behavior of the Co/TiO_2 and the $Co/Mn/TiO_2$ samples vanish completely. Therefore only the results obtained with Co/TiO_2 shall be discussed.

In the case of quantitatively running reactions there is a direct relation between the amount of the reaction gas (H_2 or O_2) consumed and the amount of metal contained in the sample, so that the oxidation state of the metal can be determined.

$$\mathrm{Co} + \frac{1}{2}\,\mathrm{O_2} \rightarrow \mathrm{CoO} \qquad \text{ratio moles } O_2\text{/moles metal} = 0.50$$

$$3\mathrm{Co} + 2\mathrm{O_2} \rightarrow \mathrm{Co_3O_4} \qquad \text{ratio moles } O_2\text{/moles metal} = 0.67.$$

When the reduced catalyst is heated under a stream of oxygen in He, oxygen is consumed at around 415, 495, and 695 K (main peak in Fig. 6a). When the heating in dilute oxygen is continued, at 1050 K a negative signal in Fig. 6a is observed; i.e., in spite of the oxidizing conditions, oxygen is formed by decomposition of an oxide. The amount of O_2 consumed below 800 K leads to a moles O_2/moles metal ratio of 0.68. At 1050 K 24% of the oxygen (ratio moles O_2/moles metal = 0.16) is again emitted. These values indicate that up to 800 K Co_3O_4 is formed, but is not stable above 1000 K, so that Co_3O_4 decomposes into CoO and O_2. To prove this hypothesis the reduced catalyst was subjected to two TPO experiments in which the highest oxidation temperatures were 773 and 1173 K, respectively. Figures 6b and 6c show the TPR curves which were observed with the reduction that followed the oxidation. In the first case (low-temperature oxidation) the TPR profile exhibits two peaks at 560 and 630 K, respectively, in agreement with the TPR profile of pure Co_3O_4 (inset to Fig. 5a), whereas in the second case (high-temperature oxidation) only one reduction peak at 975 K is observed. The moles H_2/moles metal ratio of 1.03 is in agreement with the reduction of CoO.

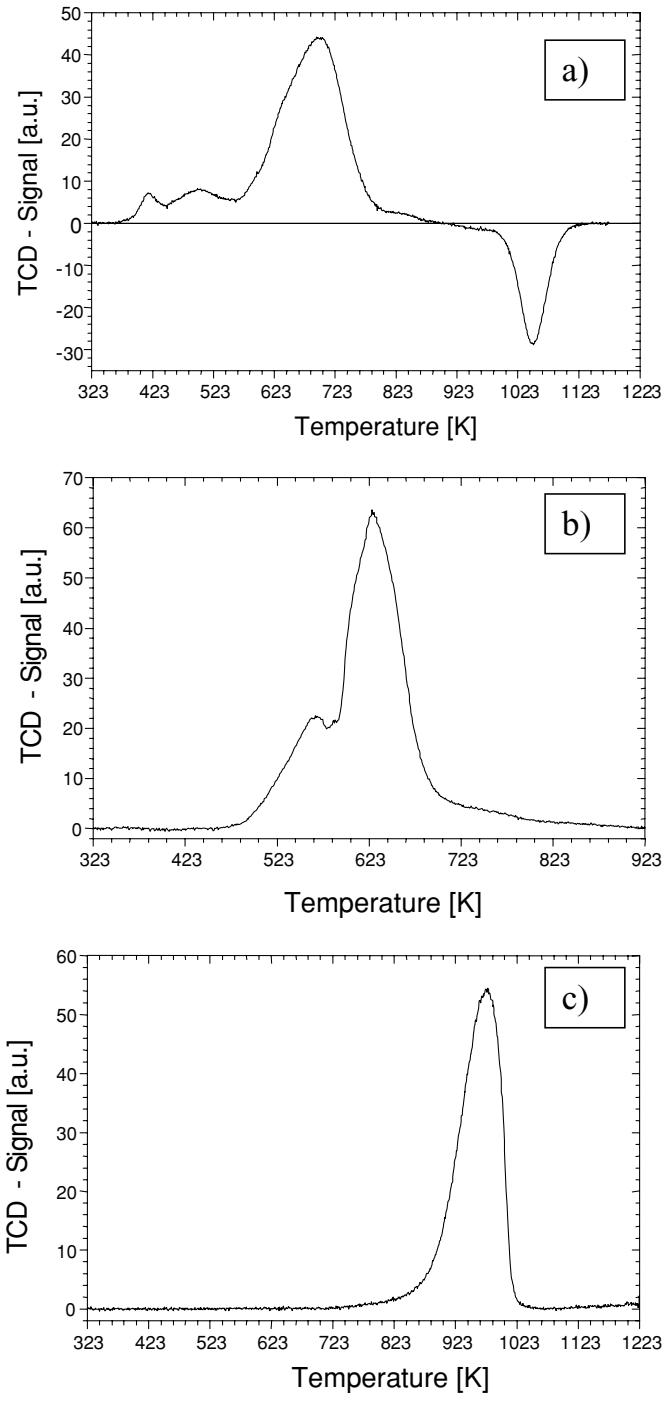

FIG. 6. (a) TPO patterns of a totally reduced Co/TiO_2 catalyst. (b) TPR experiments performed with a Co/TiO_2 catalyst after a preceding oxidation at 773 K and (c) after a preceding oxidation at 1173 K.

The position of this peak agrees rather well with the high-temperature peak, which was observed with the TPR experiments with calcined Co/TiO_2 (Fig. 5a) and calcined $Co/Mn/TiO_2$ (Fig. 5b). However, the relative intensities of these peaks differ considerably. In contrast to the TPR profile of calcined Co/TiO_2, this peak dominates the TPR profile of calcined $Co/Mn/TiO_2$. Since the XRD experiments revealed anatase and rutile as crystalline substances in both calcined catalysts and crystalline $CoTiO_3$ only in $Co/Mn/TiO_2$, it can be argued that the two valent CoO exists in the form of $CoTiO_3$ and that the reduction peak at 950 ± 30 K is characteristic of the reduction of $CoTiO_3$ to metallic Co and TiO_2. The TPO profile of Fig. 6a could then be interpreted by the equations

$$3Co^0 + 2O_2 \rightarrow Co_3O_4$$
$$\text{ratio moles } O_2/\text{moles metal} = +0.67$$
$$Co_3O_4 + 3TiO_2 \rightarrow 3CoTiO_3 + \frac{1}{2}O_2$$
$$\text{ratio moles } O_2/\text{moles metal} = -0.17.$$

Our colleagues at the Jagiellonian University have studied the oxidation and reduction of exactly the same samples (22). They used, however, other equipment, mass spectrometric detection, and slightly different experimental conditions. They arrived at similar, but not identical, plots; they find, however, deviations in the peak positions of up to 100 K compared with Figs. 5 and 6. They, too, discuss a superimposed reaction between CoO and TiO_2. This observation indicates that it is not advisable to rely on literature data, but to carry out TPR and TPO experiments with reference samples under exactly the same experimental conditions as those with the sample under investigation. In addition, it should be kept in mind that supported catalysts may change their properties during a series of oxidation/reduction cycles.

With these results in mind, it is possible to interpret the TPR curves of the calcined Co/TiO_2 and $Co/Mn/TiO_2$ samples (Figs. 5a and 5b). The moles H_2/moles metal ratio was experimentally determined to be 1.17 (Co/TiO_2) and 1.22 ($Co/Mn/TiO_2$). These values lie between those expected in the cases of Co_3O_4 and CoO reduction, respectively.

$$Co_3O_4 + 4H_2 \rightarrow 3Co^0 + 4H_2O$$
$$\text{ratio moles } H_2/\text{moles metal} = 1.33$$
$$CoO + H_2 \rightarrow Co^0 + H_2O$$
$$\text{ratio moles } H_2/\text{moles metal} = 1.00.$$

They plead for a mixture of Co^{3+} and Co^{2+}. The formation of Co_3O_4 at low temperatures is confirmed by Martens *et al.* (23), while at oxidation temperatures >800 K a higher CoO fraction is detected.

It should be mentioned that the amount of consumed H_2 excludes a reduction of manganese oxides under the given conditions. The XP spectra show that MnO exists in a highly dispersed, amorphous modification on the catalyst. Since MnO is not reducible at temperatures <700 K (11), it is assumed that MnO has no influence on the catalytic properties and serves as an additional support. This is confirmed by EXAFS and XP studies (24, 25) with Mn-doped

Co support catalysts, which were prepared by a solvated metal atom dispersed process. The authors noticed that Mn is bound to the support as a highly dispersed MnO, while Co is stabilized in a metallic form on the MnO.

To complete the TPR/TPO results the behavior of the Co/Al_2O_3 and Co/SiO_2 catalysts will be explained without figures. The calcined Co/Al_2O_3 sample shows four separated TPR maxima at 720 (species A), 820 (species B), 930 (species C), and 1060 K (species D). Compared with the Co/TiO_2 system, the signal of species A can be assigned to the reduction of CoO. But the area of peak A amounts to only 24% of the total area below the TPR curve. To identify species B–D, a TPO experiment was added. The following O_2 uptake in this experiment occurs already at 323 K, i.e., the Co/Al_2O_3 sample is significantly more reactive than Co/TiO_2 due to a higher degree of dispersion of the metallic Co. The oxidation of the catalyst comes to an end at 530 K and, as in the Co/TiO_2 system, an emission of oxygen is observed at 1100 K, likely by a reduction process from Co(III) to Co(II). TPR experiments, which were carried out after preceding oxidations up to 773 and 1173 K, demonstrate that the signals of species B and C can be assigned to the reduction of Co_3O_4 and the TPR profile D can be attributed to the reduction of $CoAl_2O_4$. Co_3O_4 on the Al_2O_3 support must be present in a highly dispersed or amorphous form, since it cannot be identified by TEM or XRD.

Other authors (26, 27) also found four TPR signals in the system Co/Al_2O_3 after a calcination temperature of 875 K. Small deviations of the peak maxima to lower and higher temperatures can likely be traced back to experimental conditions. Arnoldy and Moulijn (26) reported a reduction temperature of 590 K for bulk Co_3O_4, while other authors (28–30) discussed significantly higher temperatures in the 700 K regime.

In one TPR experiment the calcined Co/SiO_2 system shows a maximum at 630 K and a shoulder at 710 K. The oxidation signals of the totally reduced catalyst are observed at 400 and 495 K. The ratio moles O_2/moles metal = 0.63, which agrees rather well with the theoretical value of 0.67, points to a quantitative reoxidation of the metallic Co to Co_3O_4. A second TPR experiment confirms the TPO result, because the two-step reduction at 545 and 620 K is nearly identical with the TPR patterns of pure Co_3O_4 as plotted in the inset to Fig. 5a. The identification of Co_3O_4 in the Co/SiO_2 system with TPR/TPO experiments is in good agreement with the results obtained with TEM and XRD. Van't Blik *et al.* (31) discuss the formation of cobalt silicate during TPR measurement at 973 K due to the high complexity of the TPR profile. However, the preceding results exclude a strong interaction between Co_3O_4 and the support, since the reduction of the Co/SiO_2 catalyst is completely finished at 750 K. In a review (32) of metal–support interactions it was stated that transition metals form only weak van der Waals interactions with the support SiO_2. At very high temperatures (~900 K) an alloy formation to nickel silicide is possible. But such high temperatures are not reached in our experiments, and therefore a comparable formation of Co silicide or silicate can be excluded.

3.5. Results Obtained by Means of Adsorption Experiments

Both already used catalysts and newly produced catalysts were treated in the same cycle of oxidation in order to eliminate carbonaceous impurities deposited during former catalytic reactions and the same cycle of reduction to form the catalytically active metallic Co. Earlier studies of the hydrogenation of CO_2 (33, 34) have shown that this pretreatment should occur at temperatures between 593 and 683 K, which are high enough for an effective reduction of the cobalt oxides and low enough to avoid sintering. Since TPR experiments had shown that the samples could not quantitatively be reduced ($CoTiO_3$ and $CoAl_2O_4$ are stable under these conditions), it was necessary to determine the reducible fraction of the metallic component by dynamic pulse chemisorption.

Figures 7a and 7b show the results of such an experiment in the case of Co/SiO_2. The first seven oxygen pulses are

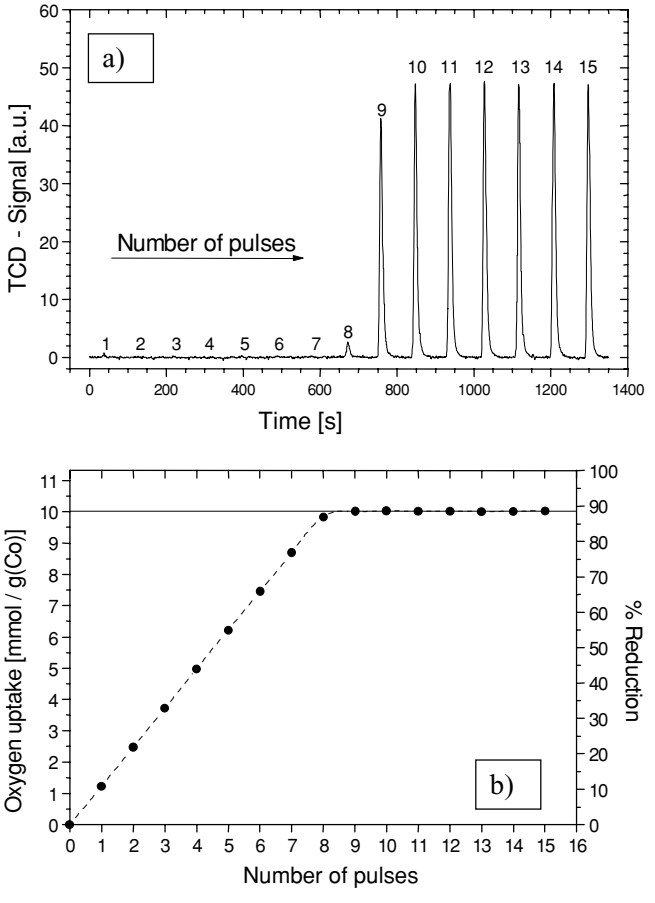

FIG. 7. (a) O_2 pulse chemisorption performed with Co/SiO_2 at $T = 673$ K and (b) O_2 uptake curve and percentage of reduction of a Co/SiO_2 catalyst as a function of the number of the O_2 pulses.

quantitatively consumed in Fig. 7a. After nine pulses the oxidation has come to an end and the pulses penetrate the sample without any change in their form. The amount of consumed oxygen can be calculated from the areas below the pulses. Comparison between the known number of Co atoms contained in the sample and the oxygen consumption allows the calculation of the degree of reduction of the catalyst. The result is plotted in Fig. 7b. The linearity of the curve in Fig. 7b also indicates that there is no significant hindrance of diffusion of oxygen during the bulk oxidation. The degree of reduction of the Co/SiO_2 catalyst amounts to about 90%.

Similar experiments, which were carried out with Co/Al_2O_3 and Co/TiO_2 catalysts, demonstrate that the specific oxygen uptake of these two catalysts at 673 K is less. Co/TiO_2 shows a degree of reduction of about 80% and Co/Al_2O_3 of only $18 \pm 2\%$ due to the nonreducible ternary compounds $CoTiO_3$ and $CoAl_2O_4$ at this temperature. Only the cobalt oxides Co_3O_4 and CoO will be reduced. These values must be considered when the degree of dispersion of the metallic Co on the various supports is calculated.

Static adsorption experiments were performed to determine the total surface area and the area of the catalytically active metallic component. From the slope and the intercept of the linearized BET isotherms the BET surfaces were calculated (35). The BET values in Table 4 reveal that the investigated catalyst samples after the calcination process show significant deviations from the producer's data. While the TiO_2 support points to an increase in the total surface area after the calcination procedure at 873 K, the Al_2O_3 and TiO_2 supports show a decrease.

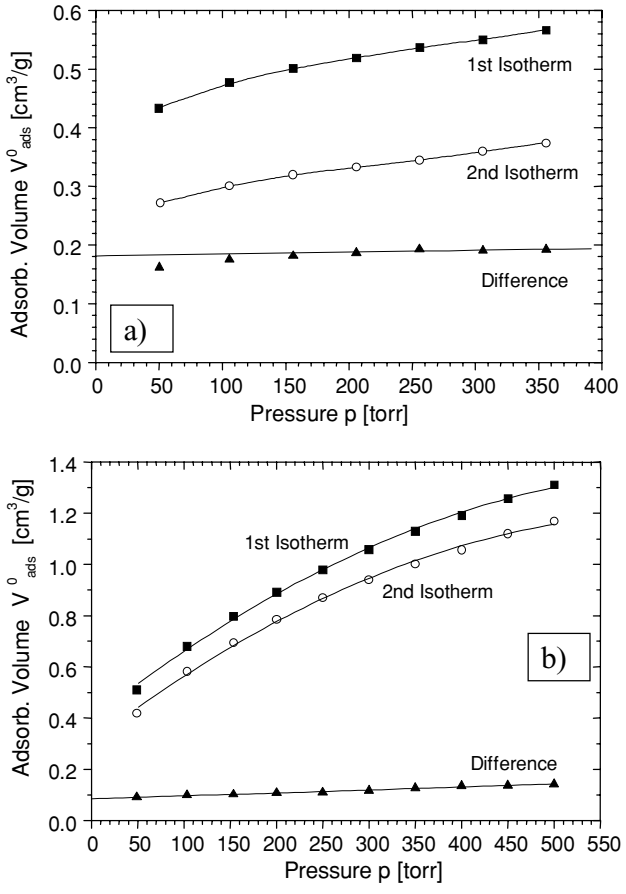

FIG. 8. Determination of the static chemisorption of (a) Co/SiO_2, $T = 323$ K, adsorbate H_2, and (b) Co/TiO_2, $T = 308$ K, adsorbate CO.

TABLE 4

Surfaces of Supported Catalysts Measured by the BET Method and Selective H_2 Chemisorption Data

	$Co/Mn/TiO_2$	Co/TiO_2	Co/Al_2O_3	Co/SiO_2
Density of the support material (g/cm^3)	3.7	3.7	2.9	2.2
Specific surface (by producers) (m^2/g)	25	25	100	200
BET surface after calcination (m^2/g)	25.4 ± 0.3	35.2 ± 0.2	85.3 ± 0.8	166.2 ± 2.3
Adsorption temperature (K)	—	308–423	373	323
Adsorbed volume $V^0_{ads.}$ (cm^3/g)	—	—	0.084	0.182
Metallic Co centers $N_{S.Co}$ (g^{-1})	—	—	9.0×10^{19}	2.1×10^{20}
Specific Co surface S_{Co} (m^2/g)	—	—	5.9	13.8
Diameter of the Co crystallites d_{Co}[a] (nm)	—	—	21	44
Degree of dispersion (%)[a]	—	—	4.9	2.3

[a] In consideration of the degree of reduction.

Selective adsorption measurements were carried out with the reduced catalysts. The procedure was the following: evacuation at 373 K for 30 min, increase in temperature up to 673 K, after 5 min reduction with H_2 at 637 K for 120 min, evacuation at 673 K for 30 min, decrease in temperature down to the adsorption temperature, and after 30 min adsorption of H_2 or CO at this temperature. For the Co/SiO_2 catalyst the first and the second hydrogen isotherms as well as their difference have been plotted in Fig. 8a. A maximum hydrogen uptake can be observed at 323 K, whereby 60% of it was physisorbed as seen from the second isotherm in Fig. 8a. From the curve temperature vs the adsorbed H_2 volume, it can be deduced that a reversible, activated process occurs. Furthermore it is known that hydrogen is dissociatively adsorbed on many transition metals (36, 37). On the other hand, the molecular CO adsorption (38) on Co/SiO_2 yields smaller and nonreproducible values for the adsorbed volume compared to hydrogen adsorption. This effect can be traced back to two different binding stoichiometries, bridged and on top bound CO molecules on Co (39–41).

The selective hydrogen chemisorption on Co/TiO_2 leads to a remarkable result: In the temperature range between

308 and 423 K no significant hydrogen chemisorption takes place after reduction of the catalyst at 673 K. It should be mentioned that such an effect has already been reported by Tauster *et al.* for supported Pt/TiO_2 catalysts (42, 43) and by Bartholomew and colleagues, who studied supported Ni/TiO_2 and Co/TiO_2 catalysts (39–41). The authors explain the small or even missing ability of the catalysts to chemisorb hydrogen by a strong metal support interaction (32, 44). On Co/Al_2O_3 about 46% of the total hydrogen amount adsorbed on the Co/SiO_2 catalyst is measured.

Also CO chemisorption on Co/TiO_2 is rather small (Fig. 8b), considerably smaller than that which can be observed with Co/Al_2O_3 or Co/SiO_2 catalysts. However, in contrast to the totally suppressed hydrogen chemisorption, a well-measurable adsorption effect is visible. The reversibly bound fraction amounts to 80–90% of the total CO uptake. Table 4 summarizes the results of the hydrogen adsorption measurements. The CO results were not taken into consideration due to the problematic adsorption geometry. The crystallite diameters for Co/Al_2O_3 and Co/SiO_2, respectively, are 21 and 44 nm and agree rather well with those determined by XRD (20–24 and 47 nm). From the XP spectra and the quantitative evaluation method after Kuipers *et al.* (19, 20) the crystallite diameter for Co/Al_2O_3 is calculated to be 17 nm, for Co/SiO_2 to be 43 nm, and for Co/TiO_2 to be 30 nm. The values obtained from XPS reveal that they are in good agreement with those obtained from other methods and the advantage of the XP method is that it delivers reliable results for all samples.

Reuel and Bartholomew (39) found a 10–11% degree of dispersion for Co/SiO_2 catalysts. The relatively-high value can be explained by the different production conditions. The samples were not calcined, but only dried and reduced under a hydrogen stream at 673 K. The calcination procedure in our experiment obviously leads to the formation of larger crystallites and a lower degree of dispersion. This result is also confirmed by studies with Ni support catalysts (40).

It should be mentioned that Co/Al_2O_3 shows a higher degree of dispersion than Co/SiO_2, although the metallic Co surface related to the total mass of the catalyst is smaller in the case of Co/Al_2O_3. The reason is that only the reducible Co amount is taken into consideration, which is significantly smaller for Co/Al_2O_3. Stranick *et al.* (45) and Reuel and Bartholomew (39) showed that the reducible part of Co/Al_2O_3 increases with increasing Co amount. Catalysts with a Co amount <1.5 % cannot be reduced in a stream of hydrogen, because the small amount of Co is totally embedded into the Al_2O_3 lattice.

4. CONCLUSIONS

The structural, chemical, and electronic properties of Co and Co/Mn catalysts supported on Al_2O_3, SiO_2, and TiO_2 were studied by a combination of different methods. Electron microscopy, X-ray diffraction, and photoelectron spectroscopy were used to investigate the calcined catalysts. Temperature-programmed reduction and oxidation and adsorption experiments completed the methods for investigating the activated catalysts.

The small interaction between Co and the SiO_2 support determines the properties of that catalyst. Crystalline Co_3O_4 with a diameter of ~45 nm is embedded in amorphous SiO_2. As a consequence of this large diameter, a relatively low dispersion of <3% is calculated. The adsorption measurements yield a BET surface of 166 m^2/g and an active metallic Co surface of 13.8 m^2/g. Only hydrogen adsorption is possible on well-defined adsorption sites, whereas CO is not well suited to use as an adsorbate due to its different adsorption stoichiometries. The degree of reduction amounts to 88%.

Co/Al_2O_3 and Co/TiO_2 form crystalline CoO in a crystalline support of γ-Al_2O_3 and TiO_2 (anatase and rutile), respectively. Small amounts of Co_3O_4 can be analyzed in Co/TiO_2, too. High-temperature phases $CoAl_2O_4$ and $CoTiO_3$ are detected by XPS and TPR, whereby the formation of $CoTiO_3$ is more strongly marked in the presence of Mn. Since these compounds are not reducible under the applied conditions, the degrees of reduction are only 18–20% (Co/Al_2O_3) and 77% (Co/TiO_2). The BET surface is 85 m^2/g and the metallic Co surface 5.9 m^2/g in the case of Co/Al_2O_3. The strong metal–support interaction prevents a determination of the Co surface by means of hydrogen adsorption in the case of Co/TiO_2, but the BET surface is determined to 35 m^2/g. The crystallite diameters can be measured in good agreement by XPS, TEM, XRD, and adsorption experiments to be 17–24 nm (Co/Al_2O_3) and 30 nm (Co/TiO_2). The highest degree of dispersion with ~5% is obtained for Co/Al_2O_3, while Co/TiO_2 lies with ~4 % between the other two catalysts.

This study has clearly shown that no method is able to provide the whole scope of information necessary to describe the properties of all catalysts. It is only the combination of different methods, which complement and support each other, that leads to reliable results.

ACKNOWLEDGMENTS

The authors thank the Fonds der Chemischen Industrie and the Max-Buchner-Stiftung for financial support. Technical help was given by the Institutes of Technical Chemistry of the Universities of Cracow and Erlangen and the Institute of Materials Science of the University of Erlangen.

REFERENCES

1. Joyner, R. W., Roberts, M. W., and Yates, K., *Surf. Sci.* **87**, 501 (1979).
2. Ruppender, H. J., Grunze, M., Kong, C. W., and Wilmers, M., *Surf. Interface Anal.* **15**, 245 (1990).
3. Dellwig, T., Rupprechter, G., Unterhalt, H., and Freund, H.-J., *Phys. Rev. Lett.* **85**, 776 (2000).

4. Kestel, U., Fröhlich, G., Borgmann, D., and Wedler, G., *Chem. Eng. Technol.* **17**, 390 (1994).
5. Klingenberg, B., Grellner, F., Borgmann, D., and Wedler, G., *Surf. Sci.* **296**, 374 (1993).
6. Grellner, F., Klingenberg, B., Borgmann, D., and Wedler, G., *Surf. Sci.* **312**, 143 (1994).
7. Grellner, F., Klingenberg, B., Borgmann, D., and Wedler, G., *J. Electron Spectrosc. Relat. Phenom.* **71**, 107 (1995).
8. Fröhlich, G., Kestel, U., Łojewska, J., Łojewski, T., Meyer, G., Voß, M., Borgmann, D., Dziembaj, R., and Wedler, G., *Appl. Catal. A: General* **134**, 1 (1996).
9. Voß, M., Fröhlich, G., Borgmann, D., and Wedler, G., *J. Catal.* **187**, 348 (1999).
10. Borgmann, D., Fröhlich, G., Kestel, U., Mex, H., Voß M., and Wedler, G., *in* "Proc. 6th ECASIA 95" (H. J. Mathieu, B. Reihl, and D. Briggs, Eds.), p. 69. Wiley, Chichester, 1995.
11. Niemantsverdriet, J. W., "Spectroscopy in Catalysis," Wiley–VCH Verlag, Weinheim, 2000.
12. Reference data were taken from the ASTM-chart and literature therein.
13. Delannay, F., Ed. "Characterization of Heterogeneous Catalysts," Dekker, New York/Basel, 1984.
14. West, A. R., "Solid State Chemistry and Its Applications," Wiley, Chichester/New York, 1984.
15. Briggs, D., and Seah, M. P., "Practical Surface Analysis," Wiley, Chichester/New York, 1990.
16. Rührnschopf, K., Thesis, University of Erlangen-Nürnberg, 1996.
17. Rührnschopf, K., Borgmann, D., and Wedler, G., *Thin Solid Film* **280**, 171 (1996).
18. Voß, M., Thesis, University of Erlangen-Nürnberg, 1998.
19. Kuipers, H. P. C. E., *Solid State Ionics* **16**, 15 (1985).
20. Kuipers, H. P. C. E., van Leuven, H. C. E., and Visser, W. M., *Surf. Interface Anal.* **8**, 235 (1986).
21. Brunauer, S., Emmett, P. H., and Teller, E., *J. Am. Chem. Soc.* **60**, 309 (1938).
22. Dziembaj, R., Łojewska, J., and Łojewski, T., *Solid State Ionics* **117,** 87 (1999).
23. Martens, J. H. A., van't Blik, H. F. J., and Prins, R., *J. Catal.* **97**, 200 (1986).
24. Tan, B. J., Klabunde, K. J., Tanaka, T., Kanai, H., and Yoshida, S., *J. Am. Chem. Soc.* **110**, 5951 (1988).
25. Tan, B. J., Klabunde, K. J., and Sherwood, P. M. A., *J. Am. Chem. Soc.* **113**, 855 (1991).
26. Arnoldy, P., and Moulijn, J. A., *J. Catal.* **93**, 38 (1985).
27. Tung, H.-C., and Yeh, C.-T., *J. Catal.* **122**, 211 (1990).
28. Brown, R., Cooper, M. E., and Whan, D. A., *Appl. Catal.* **3**, 177 (1982).
29. van't Blik, H. F. J., and Prins, R., *J. Catal.* **97**, 188 (1986).
30. Paryjczak, T., Rynkowski, J., and Karski, S., *J. Chromatogr.* **188**, 254 (1980).
31. van't Blik, H. F. J., Koningsberger, D. C., and Prins, R., *J. Catal.* **97**, 210 (1986).
32. Lamber, R., Jaeger, N., and Schulz-Ekloff, G., *Chem.-Ing.-Tech.* **63**, 681 (1991).
33. Kestel, U., Thesis, University of Erlangen-Nürnberg, 1993.
34. Fröhlich, G., Thesis, University of Erlangen-Nürnberg, 1996.
35. Boudart, M., and Djéga-Mariadassou, G., "Kinetics of Heterogeneous Catalytic Reactions," Princeton Univ. Press, Princeton, NJ, 1984.
36. Christmann, K., "Introduction to Surface Physical Chemistry" (H. Baumgärtl, E. U. Franck, and W. Grünbein, Eds.). Steinkopff Verlag, Darmstadt, 1991.
37. Černý, S., *Surf. Sci. Rep.* **26**, 1 (1996).
38. Nakamura, J., Toyoshima, I., and Tanaka, K., *Surface Sci.* **201**, 185 (1988).
39. Reuel, R. C., and Bartholomew, C. H., *J. Catal.* **85**, 63 (1984).
40. Mustard, D. G., and Bartholomew, C. H., *J. Catal.* **67**, 186 (1981).
41. Bartholomew, C. H., and Panell, R. B., *J. Catal.* **65**, 390 (1980).
42. Tauster, S. J., Fung, S. C., and Garten, R. L., *J. Am. Chem. Soc.* **100**, 170 (1978).
43. Tauster, S. J., and Fung, S. C., *J. Catal.* **55**, 29 (1978).
44. Hagen, J., "Technische Katalyse," VCH, Weinheim/New York, 1996.
45. Stranick, M. A., Houalla, M., and Hercules, D. M., *J. Catal.* **103**, 151 (1987).